LETTERS
https://doi.org/10.1038/s41567-019-0682-6

nature physics

Cooling and self-oscillation in a nanotube electromechanical resonator

C. Urgell[1,4], W. Yang[1,4*], S. L. De Bonis[1], C. Samanta[1], M. J. Esplandiu[2], Q. Dong[3], Y. Jin[3] and A. Bachtold[1*]

Nanomechanical resonators are used with great success to couple mechanical motion to other degrees of freedom, such as photons, spins and electrons[1,2]. The motion of a mechanical eigenmode can be efficiently cooled into the quantum regime using photons[2–4], but not other degrees of freedom. Here, we demonstrate a simple yet powerful method for cooling, amplification and self-oscillation using electrons. This is achieved by applying a constant (d.c.) current of electrons through a suspended nanotube in a dilution refrigerator. We demonstrate cooling to 4.6 ± 2.0 quanta of vibrations. We also observe self-oscillation, which can lead to prominent instabilities in the electron transport through the nanotube. We attribute the origin of the observed cooling and self-oscillation to an electrothermal effect. This work shows that electrons may become a useful resource for cooling the mechanical vibrations of nanoscale systems into the quantum regime.

The vibrations of mechanical resonators have been coupled to electrons in different transport regimes, such as single-electron tunnelling[5–11], Kondo[12] and the quantum Hall effect[13,14]. As mechanical resonators are excellent force sensors, a small electrostatic force created by electrons generates a large displacement of the resonator. Conversely, the displacement reacts back on the electrons by a sizeable amount. This back-action of electrons on the resonator has frequently been studied by measuring the change in resonance frequency and in the energy decay rate of vibrations[5–14]. In principle, the back-action of electrons can also be used to suppress and amplify thermal vibrational fluctuations and to generate self-oscillation by applying a d.c. electron current[15,16]. Reducing the thermal displacement fluctuations of a mechanical eigenmode is equivalent to cooling it according to the equipartition theorem. Signatures of a modest cooling to ∼200 quanta and self-oscillation were observed over a decade ago in a pioneer study[17] where a resonator was coupled to a superconducting single-electron transistor. Many theoretical schemes have been proposed to cool mechanical vibrations using electrons in different electron transport regimes[18–22]. However, these cooling schemes could not be implemented owing to experimental difficulties. Here, we show efficient back-action cooling in a current-biased suspended nanotube precooled in a dilution refrigerator.

Carbon nanotubes are a versatile system for the study of both electron transport and nanomechanics. Different electron transport regimes can be reached by tuning the transmission of electrons between the nanotube and electrodes[23]. Interaction can lead to electron attraction, Kondo behaviours and Wigner states[23–25]. As carbon nanotubes are so small, they make the lightest mechanical resonators fabricated thus far. Cooling a nanotube resonator in a dilution refrigerator leads to high quality factors[26,27]. As a result, the force sensitivity of the resonator is record-high[28], and the effect of the electron–vibration coupling is expected to be especially large.

Suspending a carbon nanotube between two metal electrodes is key to forming a nanomechanical resonator and carrying out state-of-the-art electron transport measurements. This suppresses the electron backscattering in the nanotube due to the charge impurities and the rugosity of the substrate. We grow the carbon nanotube between two metal electrodes in the last step of the fabrication process using chemical vapour deposition to minimize residual contamination[26]. Measurements are carried out by applying a d.c. voltage to the source electrode (V_{sd}) and the gate electrode (V_g) patterned at the bottom of the trench (Fig. 1a). We detect the electrical current from the drain electrode using an RLC resonator with frequency $\omega_{RLC} = 2\pi \times 1.27$ MHz and a high-electron-mobility transistor (HEMT) amplifier[28,29]. We record the differential conductance G_{diff} of the device by applying an oscillating voltage V_{sd}^{ac} to the source electrode with the frequency set at ω_{RLC}. Using a capacitive transduction scheme[28], we measure thermal vibrations with resonance frequency ω_0 by applying V_{sd}^{ac} at the frequency $\omega_0 - \omega_{RLC}$. To avoid perturbations from the measurement, we keep the amplitude of V_{sd}^{ac} much smaller than $k_B T/e$, where k_B is the Boltzmann constant, T is the temperature of the cryostat and e is the electron charge. All the measurements presented here are carried out at the base temperature of the refrigerator, except when noted otherwise.

Electron transport measurements indicate that electrons are in the Kondo regime[23]. A regular shell filling with Kondo ridges at zero source–drain bias is observed when sweeping V_g (Fig. 1b,c). Unlike a normal Coulomb blockade, G_{diff} increases in every second conductance valley when decreasing temperature. This reveals the $SU(2)$ nature of the Kondo effect in this device.

Energy decay measurements of thermal vibrations reveal that the quality factor $Q = 6.8 \times 10^6$ is remarkably high when compared with previous works[26–28]. This is also higher than the Q inferred from the spectral resonance linewidth, since the energy decay rate Γ_{decay} is smaller than the spectral resonance linewidth Γ_{width} (Fig. 1d–f). The difference is attributed to dephasing. The resonance frequency can be tuned by sweeping both V_g and V_{sd} (Fig. 1g,h). The slopes $\partial\omega_0/\partial V_g$ and $-\partial\omega_0/\partial V_{sd}$ are often similar, suggesting that they are related to the same origin—that is, the mechanical tension induced by the static displacement of the nanotube. Thermal vibrations can be cooled with the cryostat to ∼70 mK (Fig. 1i). We attribute the saturation of the displacement variance at low temperature to the electric noise in the circuit.

[1]ICFO - Institut De Ciencies Fotoniques, The Barcelona Institute of Science and Technology, Castelldefels, Spain. [2]Catalan Institute of Nanoscience and Nanotechnology, CSIC and BIST, Campus UAB, Bellaterra, Spain. [3]Centre de Nanosciences et de Nanotechnologies, CNRS, Université Paris-Sud, Université Paris-Saclay, Palaiseau, France. [4]These authors contributed equally: C. Urgell, W. Yang. *e-mail: wei.yang@icfo.eu; adrian.bachtold@icfo.eu

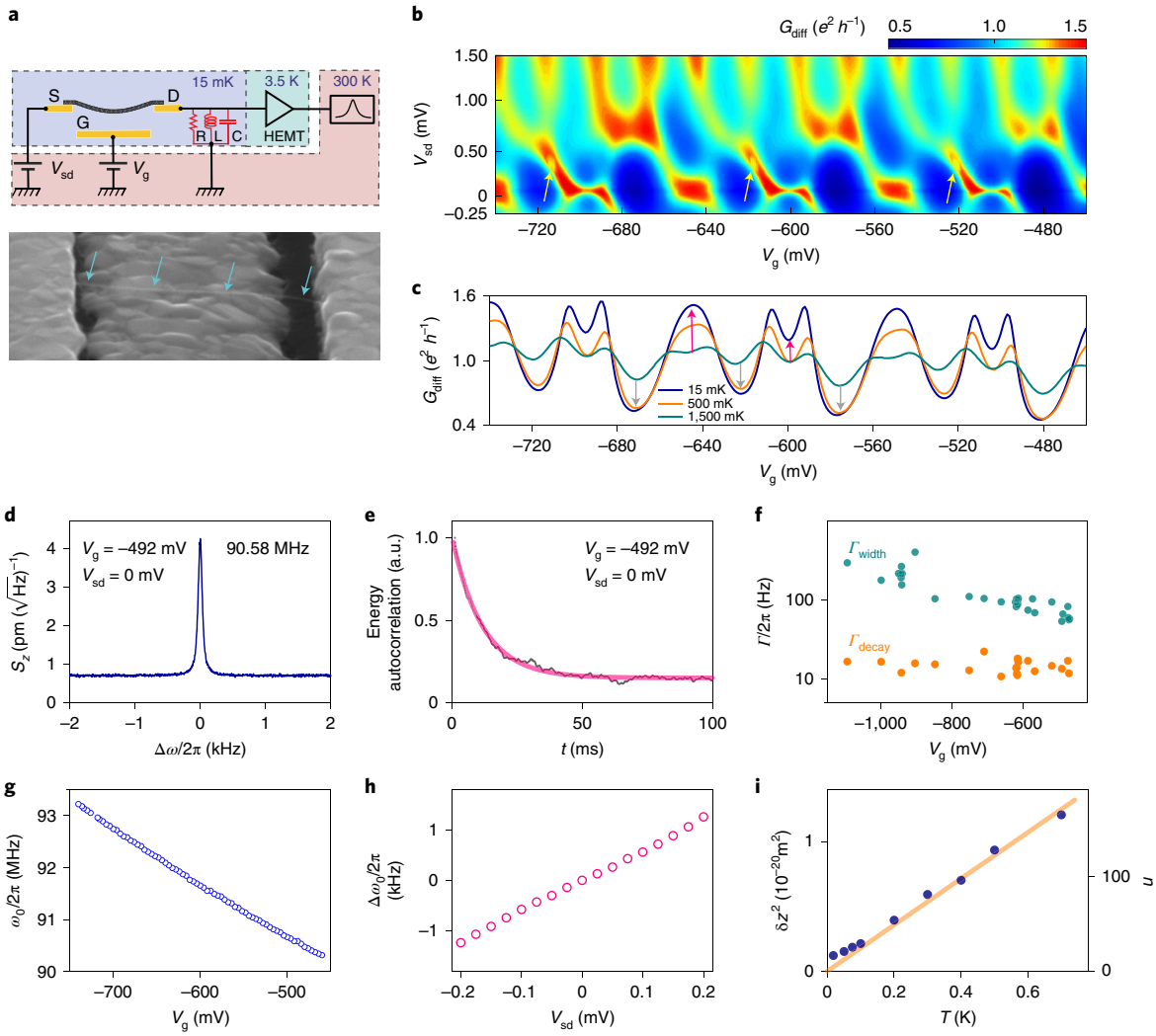

Fig. 1 | Characterization of the nanotube electromechanical resonator. a, Measurement schematic (top) and scanning electron microscopy image with tilted angle (bottom) of the suspended nanotube. The trench width is 1.1 μm. The blue arrows indicate the suspended nanotube. Voltages V_{sd} and V_g are applied to electrodes S and G, respectively. Electrode D is connected to an RLC resonator and an HEMT amplifier. **b**, G_{diff} as a function of V_{sd} and V_g. Yellow arrows indicate regions of conductance instabilities. **c**, G_{diff} as a function of V_g with $V_{sd} = 0$ mV. Upon lowering the temperature, the conductance increases and decreases as indicated by the pink and grey arrows, respectively. **d**, Displacement spectral density. **e**, Energy decay obtained from the autocorrelation of the time t trace of $X^2 + Y^2$, where X and Y are the two quadratures of thermal vibrations. The pink line indicates an exponential decay. **f**, Γ_{decay} and Γ_{width} as a function of V_g with $V_{sd} = 0$ mV. **g**,**h**, ω_0 as a function of V_g and V_{sd}. We set $V_{sd} = 0$ mV in **g** and $V_g = -560$ mV in **h**. **i**, δz^2 as a function of T at $V_g = -185$ mV; n is the quanta number.

We observe instabilities in the conductance arising periodically in V_g (see arrows in Fig. 1b). They emerge at a finite source–drain bias in charge stability diagram measurements. In these instability regions, the peaks in conductance are truncated (Fig. 2a–c), and conductance traces as a function of V_g seem noisy (Fig. 2d). While similar conductance instabilities were previously reported[8], we show that these instabilities are related to large-amplitude vibrations.

The measured conductance instabilities originate from switching the mechanical motion between thermal noise and self-oscillation (Fig. 3). On sweeping V_{sd} through the instability region, the variance of the displacement δz^2 dramatically increases (Fig. 3a), and the decay rate is suppressed towards zero near the border of the instability region (shaded in yellow in Fig. 3b). These two experimental facts point to the development of self-oscillation. The phase space and the histogram of the two quadratures of the motion can be described by the superposition of the distributions of a doughnut and a Gaussian-like peak (Fig. 3h,i), suggesting that the motion switches back and forth between self-oscillation with high δz^2 and thermal noise with low δz^2 (Supplementary Information Section III). This switching is further supported by the fact that the resonance lineshape is unusually broad (Fig. 3g); indeed, the large linewidth is then related to the large fluctuations of δz^2 and the resonator nonlinearity. Pure self-oscillation with a narrow resonance lineshape can also be observed without any switches to thermal vibrations; this often happens at higher V_{sd} values. The shift in resonance frequency due to electron back-action (Fig. 3c) is difficult to quantify, since the resonance frequency also depends on the mechanical tension induced by V_{sd}, the temperature rise of the nanotube lattice due to Joule heating and the variance of the displacement through the mechanical nonlinearity.

Mechanical vibrations are cooled to 4.6 ± 2.0 quanta at $V_g = -943$ mV when the source–drain bias voltage is increased to $V_{sd} = 0.565$ mV (Fig. 4a–c). Cooling is accompanied by a strong increase in the decay rate (Fig. 4d), indicating a back-action effect.

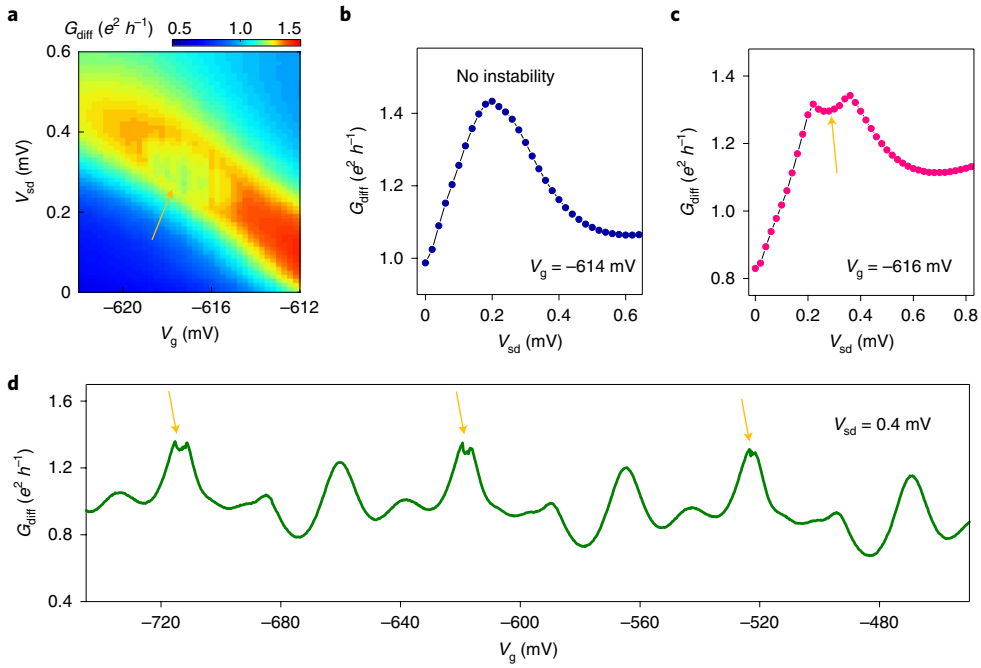

Fig. 2 | Conductance instabilities. a, G_{diff} as a function of V_{sd} and V_g. Yellow arrows in the different panels indicate regions of conductance instability. **b**,**c**, G_{diff} as a function of V_{sd} for $V_g = -614$ mV (**b**) and $V_g = -616$ mV (**c**). **d**, G_{diff} as a function of V_g.

This efficient cooling occurs when the transconductance is negative and large (Fig. 4e). We observe cooling at other V_g values when the transconductance is also negative (Supplementary Information Section II). The determination of the number of quanta is robust against the hypothetical miscalibration of the amplification chain and of the attenuation along the coaxial cables (see Methods). The uncertainty in the transconductance, which enters into the transduction of the displacement, is 5.7% of its value at $V_g = -943$ mV and $V_{sd} = 0.565$ mV. As explained above, the frequency shift due to back-action cannot be quantified, since the frequency shift depends on various other effects that are difficult to disentangle experimentally.

The nanotube experiences Joule heating due to the current flowing through the resonator. Back-action cooling predicts that the phonon occupation at finite bias is given by $n(V_{sd}) = \Gamma_{bath} n_{bath}/\Gamma_{decay}(V_{sd})$ where $n_{bath} = k_B T_{bath}/\hbar\omega_0$ is the thermal phonon number and Γ_{bath} is the coupling to the thermal bath. We would achieve much lower phonon occupation if the bath temperature T_{bath} was given by the cryostat temperature, while setting Γ_{bath} to the measured decay rate at zero bias. This indicates that Joule heating is sizable. We deduce T_{bath} from the measured values of n and Γ_{decay} (Fig. 4f)[30,31]. The temperature rise can be well described by Joule heating for different V_g values using the phenomenological relation $T_{bath} = T^0_{vib} + \eta G V^2_{sd}$ (Fig. 4f), where T^0_{vib} is the measured vibration temperature at zero bias, G is the conductance and η is a free parameter that we take to be constant for all the V_g values. The temperature rise is not accounted for by the electrostatic force associated with the electron shot noise of the nanotube, since the temperature rise does not depend linearly on V_{sd} and is independent of V_g to a first approximation. The shot noise of the suspended nanotube behaves in the usual way with a Fano factor between 0.2 and 0.3 (Supplementary Information Section IV).

Here, we discuss the possible origins of the observed back-action. It could be related to the usual back-action in electromechanical resonators[5–12], where conducting electrons generate an electrostatic force on the nanotube, and the retardation of the force is due to the transmission of electrons between the nanotube and the electrodes. However, we do not observe resonance frequency dips when sweeping V_g (Fig. 1g), showing that the strength of this back-action is weak. Moreover, this back-action predicts modest cooling at the conductance peaks[15,16], which is the opposite of what is observed in Fig. 2, that is, self-oscillation near conductance peaks. This shows that the back-action measured in electromechanical resonators at zero source–drain bias cannot describe our results at finite bias. Another possible mechanism could be related to the retardation created by the circuit, where the vibration-induced current noise of the nanotube generates a retarded electrostatic force due to the capacitance of the circuit. However, the predicted decay rate is too weak to produce the cooling observed in Fig. 4a,c. We conclude that back-action with electrostatic origins cannot account for our findings.

We attribute the origin of the back-action to an electrothermal effect[32], which is an analogue of the photothermal back-action often observed in optomechanical resonators[33]. The power GV^2_{sd} of Joule heating modifies the mechanical tension in the nanotube through the effective thermal expansion coefficient of the device. This results in a net displacement δz of the resonator when the nanotube is bent by the static electrostatic force associated with V_g, for example. This displacement reacts back on the dissipated power via $\delta G = \frac{dG}{dz}\delta z$ with a delay given by both the capacitance of the circuit and the thermalization time of the device[32]. This electrothermal effect modifies the decay rate by

$$\Delta\Gamma_{back} = -\alpha \frac{dG_{diff}}{dV_g} \frac{C'_g}{C_g} V_g z_s V^2_{sd} \qquad (1)$$

Here, C_g is the capacitance between the nanotube and the gate electrode, C'_g is its derivative with respect to z and z_s is the static displacement. We use α as a free parameter in our analysis, since α depends on various quantities that are difficult to quantify such as the thermalization time, the effective thermal expansion coefficient and the three-dimensional profile of the static bending of the nanotube.

The electron transport in the device controls the electrothermal back-action through $\frac{dG_{diff}}{dV_g}$. When $\frac{dG_{diff}}{dV_g}$ is positive and large, the total decay rate of the resonator can become effectively negative,

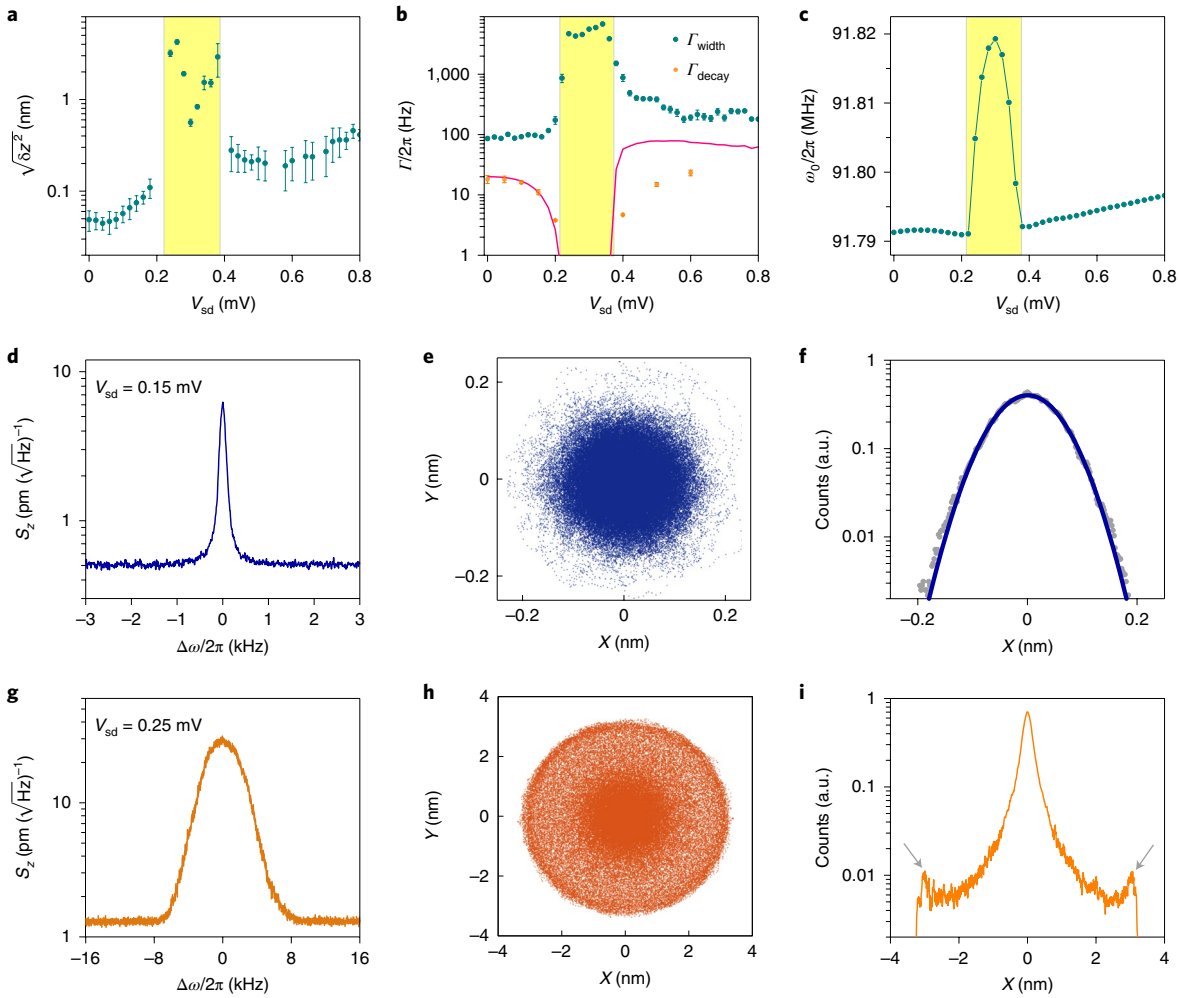

Fig. 3 | Self-oscillation at $V_g = -616$ mV. a, δz^2 as a function of V_{sd}. The yellow shaded area represents the region with self-oscillation. **b**, Γ_{decay} and Γ_{width} as a function of V_{sd}. The pink line is the expected decay rate using equation (1). **c**, ω_0 as a function of V_{sd}. **d–f**, S_z (**d**), the phase space of the two quadratures of the motion (**e**) and the associated histogram (**f**) at $V_{sd} = 0.15$ mV. **g–i**, S_z (**g**), the phase space of the two quadratures of the motion (**h**) and the associated histogram (**i**) at $V_{sd} = 0.25$ mV. The arrows in **i** indicate the doughnut distribution. The confidence interval error bars in **a** and **b** arise from the uncertainty in the fitting of the measurement of the resonance lineshape and the energy decay to a Lorentzian and an exponential decay, respectively.

leading to self-oscillation. When $\frac{dG_{diff}}{dV_g}$ is strongly negative so that $\Delta\Gamma_{back} \gg \Gamma_{bath}$, the vibrations are efficiently cooled. Equation (1) qualitatively reproduces the decay rate measured when increasing V_{sd} towards the self-oscillation regime shaded in yellow in Fig. 3b and to the strong cooling regime in Fig. 4d (see pink lines). See Section VI of the Supplementary Information for more discussion on the different back-actions.

Our detection method enables excellent displacement sensitivity. The imprecision noise S_z^{imp} can reach the level of the displacement noise of the zero-point fluctuations at resonance frequency, $S_z^{zpf} = \sqrt{2\hbar/m\omega_0\Gamma_{width}}$, where m is the effective mass (Supplementary Information Section. V) and $\hbar$ is the reduced Planck constant. The imprecision noise in this detection scheme can be further suppressed by setting the device transconductance to a higher value, while keeping the electron shot noise to a lower level compared with the Johnson–Nyquist noise by applying the source–drain voltage bias below $k_B T$. The imprecision noise reads

$$S_z^{imp} = \left(\frac{1}{2}\frac{dG_{diff}}{dV_g} V_g V_{sd}^{ac} \frac{C_g'}{C_g}\right)^{-1} S_I^{imp} \qquad (2)$$

Here S_I^{imp} is the current noise floor associated with the HEMT amplifier noise, the Johnson–Nyquist noise of the circuit and the electron shot noise through the nanotube device, which can be tuned by V_{sd}^{ac} and V_{sd}.

Electrothermal cooling is a striking effect, since it takes advantage of Joule heating to cool mechanical vibrations. This cooling mechanism is also efficient at temperatures close to the quantum regime. The electrothermal cooling method is simple, as it consists of applying a direct current of electrons through a suspended nanoelectronic device. Our measurements of thermal vibrations are similar to the noise measurements on electronic devices obtained by others[34–36]. Electrothermal cooling allows us to demonstrate the lowest occupation number achieved with a resonator based on a low-dimensional nanoscale material[28,30,31,33]. Future studies may enable ground-state cooling achieved by enhancing the back-action rate (equation (1)) using devices with higher transconductance and stronger coupling to the gate (to increase the C_g'/C_g ratio). It will then be interesting to investigate the lowest measurement noise related to the imprecision noise and the quantum back-action noise, which arises from the electrostatic force noise associated with the electron shot noise. Cooling is also promising for enhancing the polaronic nature of

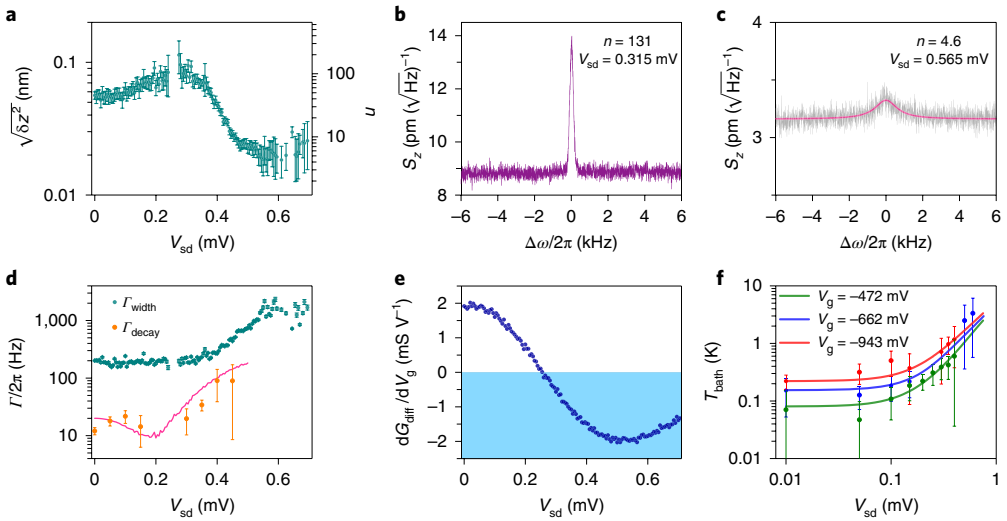

Fig. 4 | Cooling at $V_g = -943$ mV. a, δz^2 as a function of V_{sd}. **b**,**c**, S_z at $V_{sd} = 0.315$ mV (**b**) and $V_{sd} = 0.565$ mV (**c**). **d**, Γ_{decay} and Γ_{width} as a function of V_{sd}. The pink line is the expected decay rate using equation (1). **e**, Transconductance as a function of V_{sd}. The blue shading indicates the region with negative transconductance. **f**, T_{bath} of mechanical vibrations as a function of V_{sd} for three different V_g values. The solid lines indicate the dependence expected from Joule heating. The confidence interval error bars in **a** and **d** arise from the uncertainty in the fitting of the measurement of the resonance lineshape and the energy decay to a Lorentzian and an exponential decay, respectively. The error bars in **f** arise from the uncertainties in δz^2 and Γ_{decay}.

charge carriers in a single-electron tunnelling device[37]. This might offer the possibility of tuning the zero-frequency electrical conduction of an electromechanical device.

Online content

Any methods, additional references, Nature Research reporting summaries, source data, statements of code and data availability and associated accession codes are available at https://doi.org/10.1038/s41567-019-0682-6.

Received: 11 March 2019; Accepted: 5 September 2019;
Published online: 7 October 2019

References

1. Treutlein, P., Genes, C., Hammerer, K., Poggio, M. & Rabl, P. *Hybrid Mechanical Systems* (Springer, 2014).
2. Aspelmeyer, M., Kippenberg, T. J. & Marquardt, F. Cavity optomechanics. *Rev. Mod. Phys.* **86**, 1391–1452 (2014).
3. Clark, J. B., Lecocq, F., Simmonds, R. W., Aumentado, J. & Teufel, J. D. Sideband cooling beyond the quantum backaction limit with squeezed light. *Nature* **541**, 191–195 (2017).
4. Rossi, M., Mason, D., Chen, J., Tsaturyan, Y. & Schliesser, A. Measurement-based quantum control of mechanical motion. *Nature* **563**, 53–58 (2018).
5. Knobel, R. G. & Cleland, A. N. Nanometre-scale displacement sensing using a single electron transistor. *Nature* **424**, 291–293 (2003).
6. Woodside, M. T. & McEuen, P. L. Scanned probe imaging of single-electron charge states in nanotube quantum dots. *Science* **296**, 1098–1101 (2002).
7. Lassagne, B., Tarakanov, Y., Kinaret, J., Garcia-Sanchez, D. & Bachtold, A. Coupling mechanics to charge transport in carbon nanotube mechanical resonators. *Science* **325**, 1107–1110 (2009).
8. Steele, G. A. et al. Strong coupling between single-electron tunneling and nanomechanical motion. *Science* **325**, 1103–1107 (2009).
9. Benyamini, A., Hamo, A., Kusminskiy, S. V., von Oppen, F. & Ilani, S. Real-space tailoring of the electron–phonon coupling in ultraclean nanotube mechanical resonators. *Nat. Phys.* **10**, 151–156 (2014).
10. Ares, N. et al. Resonant optomechanics with a vibrating carbon nanotube and a radio-frequency cavity. *Phys. Rev. Lett.* **117**, 170801 (2016).
11. Okazaki, Y., Mahboob, I., Onomitsu, K., Sasaki, S. & Yamaguchi, H. Gate-controlled electromechanical backaction induced by a quantum dot. *Nat. Commun.* **7**, 11132 (2016).
12. Götz, K. J. G. et al. Nanomechanical characterization of the Kondo charge dynamics in a carbon nanotube. *Phys. Rev. Lett.* **120**, 246802 (2018).
13. Singh, V. et al. Coupling between quantum Hall state and electromechanics in suspended graphene resonator. *Appl. Phys. Lett.* **100**, 233103 (2012).
14. Chen, C. et al. Modulation of mechanical resonance by chemical potential oscillation in graphene. *Nat. Phys.* **12**, 240–244 (2016).
15. Clerk, A. A. & Bennett, S. Quantum nanoelectromechanics with electrons, quasi-particles and cooper pairs: effective bath descriptions and strong feedback effects. *New J. Phys.* **7**, 238 (2005).
16. Armour, A. D., Blencowe, M. P. & Zhang, Y. Classical dynamics of a nanomechanical resonator coupled to a single-electron transistor. *Phys. Rev. B* **69**, 125313 (2004).
17. Naik, A. et al. Cooling a nanomechanical resonator with quantum back-action. *Nature* **443**, 193–196 (2006).
18. Zippilli, S., Morigi, G. & Bachtold, A. Cooling carbon nanotubes to the phononic ground state with a constant electron current. *Phys. Rev. Lett.* **102**, 096804 (2009).
19. Santandrea, F., Gorelik, L. Y., Shekhter, R. I. & Jonson, M. Cooling of nanomechanical resonators by thermally activated single-electron transport. *Phys. Rev. Lett.* **106**, 186803 (2011).
20. Stadler, P., Belzig, W. & Rastelli, G. Ground-state cooling of a carbon nanomechanical resonator by spin-polarized current. *Phys. Rev. Lett.* **113**, 047201 (2014).
21. Arrachea, L., Bode, N. & von Oppen, F. Vibrational cooling and thermoelectric response of nanoelectromechanical systems. *Phys. Rev. B* **90**, 125450 (2014).
22. Stadler, P., Belzig, W. & Rastelli, G. Ground-state cooling of a mechanical oscillator by interference in Andreev reflection. *Phys. Rev. Lett.* **117**, 197202 (2016).
23. Laird, E. A. et al. Quantum transport in carbon nanotubes. *Rev. Mod. Phys.* **87**, 703–764 (2015).
24. Hamo, A. et al. Electron attraction mediated by Coulomb repulsion. *Nature* **535**, 395–400 (2016).
25. Deshpande, V. V. & Bockrath, M. The one-dimensional Wigner crystal in carbon nanotubes. *Nat. Phys.* **4**, 314–318 (2008).
26. Moser, J., Eichler, A., Güttinger, J., Dykman, M. I. & Bachtold, A. Nanotube mechanical resonators with quality factors of up to 5 million. *Nat. Nanotechnol.* **9**, 1007–1011 (2014).
27. Hüttel, A. K. et al. Carbon nanotubes as ultrahigh quality factor mechanical resonators. *Nano Lett.* **9**, 2547–2552 (2009).
28. de Bonis, S. L. et al. Ultrasensitive displacement noise measurement of carbon nanotube mechanical resonators. *Nano Lett.* **18**, 5324–5328 (2018).
29. Khivrich, I., Clerk, A. A. & Ilani, S. Nanomechanical pump–probe measurements of insulating electronic states in a carbon nanotube. *Nat. Nanotechnol.* **14**, 161–167 (2019).
30. Song, X., Oksanen, M., Li, J., Hakonen, P. J. & Sillanpää, M. A. Graphene optomechanics realized at microwave frequencies. *Phys. Rev. Lett.* **113**, 027404 (2014).
31. Weber, P., Güttinger, J., Noury, A., Vergara-Cruz, J. & Bachtold, A. Force sensitivity of multilayer graphene optomechanical devices. *Nat. Commun.* **7**, 12496 (2016).

32. Steeneken, P. G. et al. Piezoresistive heat engine and refrigerator. *Nat. Phys.* **7**, 354–359 (2011).
33. Barton, R. A. et al. Photothermal self-oscillation and laser cooling of graphene optomechanical systems. *Nano Lett.* **12**, 4681–4686 (2012).
34. Bocquillon, E. et al. Coherence and indistinguishability of single electrons emitted by independent sources. *Science* **339**, 1054–1057 (2013).
35. Jullien, T. et al. Quantum tomography of an electron. *Nature* **514**, 603–607 (2014).
36. Banerjee, M. et al. Observation of half-integer thermal Hall conductance. *Nature* **559**, 205–210 (2018).
37. Pistolesi, F. & Labarthe, S. Current blockade in classical single-electron nanomechanical resonator. *Phy. Rev. B* **76**, 165317 (2007).

Acknowledgements

We thank M. Dykman, F. Pistolesi and D. Chang for discussions. This work is supported by ERC advanced grant number 692876, the Cellex Foundation, the CERCA Programme, AGAUR (grant number 2017SGR1664), Severo Ochoa (grant number SEV-2015-0522), MICINN grant number RTI2018-097953-B-I00 and the Fondo Europeo de Desarrollo Regional. We thank B. Thibeault at UCSB for fabrication help.

Author contributions

W.Y. fabricated the devices with the support of C.U. and M.J.E. in the growth. C.U. and W.Y. carried out the measurements. C.U., W.Y., S.L.B., C.S., Q.D. and Y.J developed the detection circuit. C.U., W.Y. and A.B. analysed the data and wrote the manuscript. A.B. supervised the work.

Competing interests

The authors declare no competing interests.

Additional information

Supplementary information is available for this paper at https://doi.org/10.1038/s41567-019-0682-6.

Correspondence and requests for materials should be addressed to W.Y. or A.B.

Methods

Detection of mechanical vibrations. Electron–vibration coupling not only leads to back-action[5–14,38–43] but also enables the detection of vibrations[26–29,44]. Mechanical vibrations are electrically detected using an RLC resonator and a HEMT amplifier cooled at liquid-helium temperature (Fig. 1a)[28]. Displacement modulation is transduced capacitively into current modulation by applying an input oscillating voltage V_{sd}^{ac} across the nanotube. The frequency $\omega_{sd}/2\pi$ of the oscillating voltage is set to match $\omega_{sd}=\omega_0\pm\omega_{RLC}$. Thermal vibrations are measured by recording the current noise at $\sim\omega_{RLC}$. The current δI is related to the displacement of the nanotube by

$$\delta I = \beta\delta z \tag{3}$$

where the constant β is

$$\beta = \frac{1}{2}\frac{dG_{diff}}{dV_g}V_g V_{sd}^{ac}\frac{C_g'}{C_g} \tag{4}$$

The spectral density S_z of the displacement noise is obtained from the measured spectral density of the current noise using equations (3) and (4).

The equipartition theorem is used to reliably calibrate the number of quanta:

$$m\omega_0^2\delta z^2 = k_B T \tag{5}$$

In practice, we measure the spectral density of the current noise to quantify the variance of the current δI_{res}^2 associated to the mechanical resonance of thermal vibrations. The measurement of δI_{res}^2 as a function of temperature in Fig. 1i determines $m\left(\frac{C_g}{C_g'}\right)^2 = 2.5\times10^{-33}\,\mathrm{kg\,m^2}$ using equations (3)–(5). This allows us to quantify the effective temperature of the thermal vibrations T_{vib} at any V_g and V_{sd} by measuring δI_{res}^2 and $\frac{dG_{diff}}{dV_g}$ and using

$$T_{vib} = m\left(\frac{C_g}{C_g'}\right)^2\frac{4\omega_0^2}{k_B\left(\frac{dG_{diff}}{dV_g}V_g V_{sd}^{ac}\right)^2}\delta I_{res}^2 \tag{6}$$

The determination of T_{vib} does not depend on the hypothetical inaccurate calibration of the attenuation along the coaxial cables created by thermal contraction and of the amplification chain. Indeed, such inaccurate calibration, if sizeable, would have an effect on V_{sd}^{ac} and $m\left(\frac{C_g}{C_g'}\right)^2$, but it would be cancelled out when determining T_{vib}. We systematically measure $\frac{dG_{diff}}{dV_g}$ at any V_{sd} and V_g. The number of quanta of vibrations is obtained using $n = \frac{k_B T_{vib}}{\hbar\omega_0} - \frac{1}{2}$.

Γ_{decay} is estimated by measuring the time trace of the two quadratures of thermal vibrations and by quantifying the autocorrelation of the amplitude squared. From these time trace measurements, we also obtain the phase space of the two quadratures and the associated histogram (Fig. 3).

Data availability

The data represented in Figs. 1b, 2a, 3 and 4 are available as Supplementary Data 1–4. All other data that support the plots within this paper and other findings of this study are available from the corresponding authors on reasonable request.

References

38. Zhu, J., Brink, M. & McEuen, P. L. Frequency shift imaging of quantum dots with single-electron resolution. *Appl. Phys. Lett.* **87**, 242102 (2005).
39. Stomp, R. et al. Detection of single-electron charging in an individual InAs quantum dot by noncontact atomic-force microscopy. *Phys. Rev. Lett.* **94**, 056802 (2005).
40. LaHaye, M. D., Suh, J., Echternach, P. M., Schwab, K. C. & Roukes, M. L. Nanomechanical measurements of a superconducting qubit. *Nature* **459**, 960–964 (2009).
41. Bennett, S. D., Cockins, L., Miyahara, Y., Grütter, P. & Clerk, A. A. Strong electromechanical coupling of an atomic force microscope cantilever to a quantum dot. *Phys. Rev. Lett.* **104**, 017203 (2010).
42. Pirkkalainen, J.-M. et al. Cavity optomechanics mediated by a quantum two-level system. *Nat. Commun.* **6**, 6981 (2015).
43. Deng, G.-W. et al. Strongly coupled nanotube electromechanical resonators. *Nano Lett.* **16**, 5456–5462 (2016).
44. Sazonova, V. et al. A tunable carbon nanotube electromechanical oscillator. *Nature* **431**, 284–287 (2004).